Three-Phase Weinberg Isolated DC–DC Converter: Analysis, Design, and Experimentation

Hugo R. E. Larico and Ivo Barbi, *Fellow, IEEE*

***Abstract*—This paper presents the three-phase version of the isolated dc–dc Weinberg converter. The main characteristics of the proposed converter are as follows: small volume, low weight, reduced number of components, buck operation for a duty cycle of less than 1/3, and input and output current ripple cancellation for a duty cycle of 1/3 or 2/3. Typical applications include telecommunication, electric vehicles, renewable energy conversion systems, and batteries. This paper gives theoretical analysis, design example, and experimental data on a 735-W 120-Vdc-input 75-Vdc-output 42-kHz switching frequency laboratory prototype. The prototype performance shows good agreement with the theoretical predictions.**

***Index Terms*—Current fed, push–pull, three-phase dc–dc converter, Weinberg.**

I. Introduction

THE association of high efficiency and high current is the major problem related to low-voltage high-power applications, particularly when they require isolation at high frequency, resulting in high conduction losses. The family of push–pull converters [1]–[12], which presents a reduced number of components, allows low conduction losses, increasing the efficiency of the converter.

Push–pull converters can be classified as voltage fed or current fed. The voltage-fed type is a step-down converter which is employed for low and medium current levels, whereas the current-fed push–pull converter is preferable for high current levels since its high-frequency transformer does not present the saturation problem. However, the latter is a step-up converter, and if the application requires a step-down (buck-type) converter without the transformer saturation problem, then the Weinberg converter, shown in Fig. 1, represents a suitable option.

This paper presents the three-phase Weinberg isolated dc–dc converter, which is shown in Fig. 2. This proposed converter merges the main characteristics of the three-phase topologies [13]–[22] and the Weinberg circuit, resulting in the following advantages:

1) low conduction losses, since there is only a single device voltage drop at the input and the output sides;
2) reduced number of components: three transistors (S1–S3), four diodes (D1–D4), a three-phase transformer (T), a coupled inductor (L_f), and a filter capacitor (C_o);

Manuscript received June 16, 2010; revised January 10, 2011 and April 13, 2011; accepted April 17, 2011. Date of publication May 5, 2011; date of current version October 18, 2011.

The authors are with the Department of Electrical Engineering, Federal University of Santa Catarina (UFSC), 88040-970 Florianópolis, Brazil (e-mail: estofanero@inep.ufsc.br; ivobarbi@inep.ufsc.br).

Digital Object Identifier 10.1109/TIE.2011.2151814

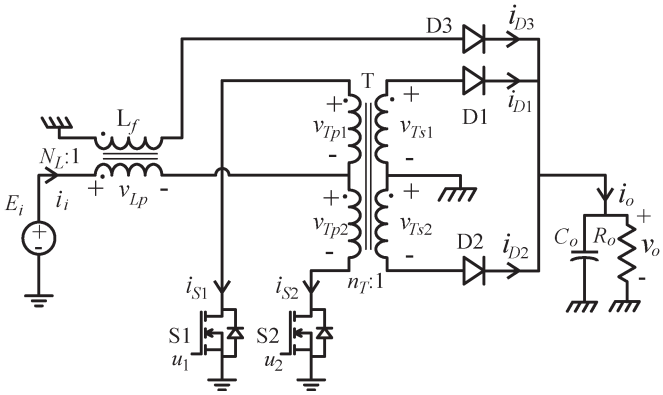

Fig. 1. Weinberg dc–dc converter.

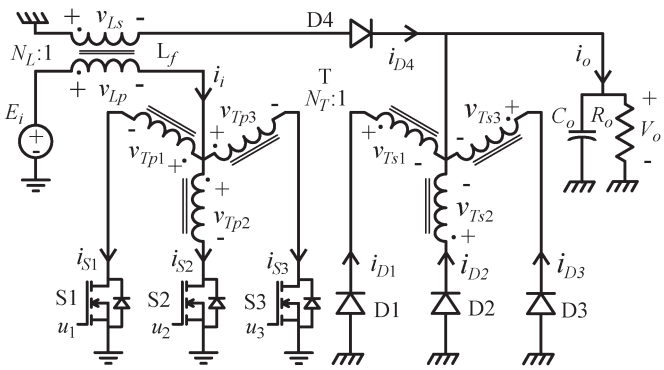

Fig. 2. Three-phase Weinberg dc–dc converter.

3) good transformer copper and core utilization;
4) connection of the transistors to the same reference point, thus allowing them to be directly driven;
5) small filter sizes $(L_f$ and $C_o)$ since the frequencies of voltage and current waves are three times the switching frequency;
6) fast response times;
7) absence of flux-imbalance problem in the high-frequency three-phase transformer, because there is a high impedance (inductor L_f) between the input and the transformer;
8) high-power processing, since the three-phase system allows a decrease in the current stresses in power devices.

The proposed topology can be operated with overlapping and nonoverlapping conduction of transistors. For $N_L = 2N_T$ (inductor and transformer turn ratios) and a duty cycle ranging from 0 to 1/3, the converter operates as a step-down converter. In this case, the output current is continuous, and the theoretical static gain is $V_o/E_i = 3D/2N_T$.

In applications where output voltage regulation is not required, the operation with a duty cycle of 1/3 allows the reactive energy minimization in the converter; therefore, a high efficiency can be obtained.

II. Theoretical Operation

The following assumptions are made to simplify the theoretical description of the operating principle.

1) The operation is in steady state.
2) The magnetic flux in the inductor core is continuous.
3) All switching elements are ideal.
4) The capacitance of capacitor C_o is large enough for the output voltage ripple to be neglected.
5) The windings of the inductor L_f (or flyback transformer) and of the three-phase transformer T are tightly coupled and have a negligible resistance.
6) The three-phase transformer is symmetrical, and its magnetization current is negligible.
7) The power transistors are symmetrically driven using the three-phase gating signals, as shown in Fig. 5.

The output voltage V_o is regulated employing pulsewidth modulation in order to control the duty cycle ($D = t_{\rm on}/T_s$), which is defined as the ratio between *on* time ($t_{\rm on}$) and *switching* period (T_s). The duty cycle of each transistor can be varied from 0% to 100%.

This paper addresses the operation in continuous conduction mode (CCM) for a duty cycle varying from 0 to 1/3, where the transistors operate in the nonoverlapping conduction mode ($t_{\rm on} < T_s/3$).

A. Principle of Operation

In CCM, the input current is discontinuous, but the output current is continuous, since the electrical power is always transferred to the output load from the inductor or from the input source through the three-phase transformer.

There are six stages in a duty cycle. In the first, third, and fifth stages, the input source provides energy to the circuit, and some of this is stored in the inductor. In the second, fourth, and sixth stages, the energy stored in the inductor is transferred to the load, and no energy is supplied from the input source. Analysis of the first and second stages is sufficient to describe the complete operation of the three-phase Weinberg converter, since the transistors are sequentially gated.

1) First Stage $[t_0, t_1]$*:* The equivalent circuit of this stage is shown in Fig. 3, where L_m is the magnetizing inductance of the inductor. This stage starts at instant t_0, when the transistor S1 is turned on and D4 is reverse biased. The inductor magnetizing current (i_m) flows through the primary winding of phase 1 which results in D2 and D3 being forward biased. The output voltage is then applied to the secondary windings of phases 2 and 3 ($V_{\rm Ts2} = V_{\rm Ts3} = -V_o$), and therefore, the voltage across the active primary winding is $2N_TV_o$. Thus, the inductor stores energy through its primary winding with a voltage of $v_{\rm Lp} = E_i - 2N_TV_o$. The voltage across transistors S2 and S3 is $3N_TV_o$. The reverse voltage across D1 is $3V_o$. The current across D2 and D3 is $i_{D2} = i_{D3} = N_Ti_i$.

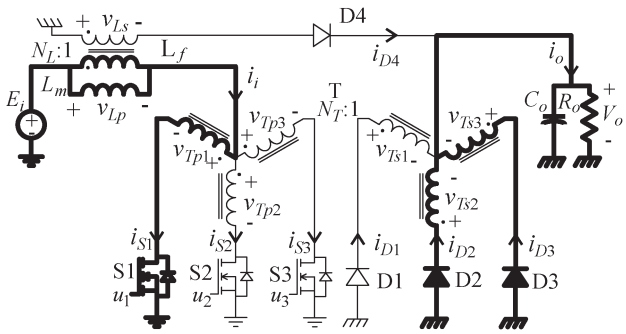

Fig. 3. Equivalent circuit of first stage $[t_0, t_1]$.

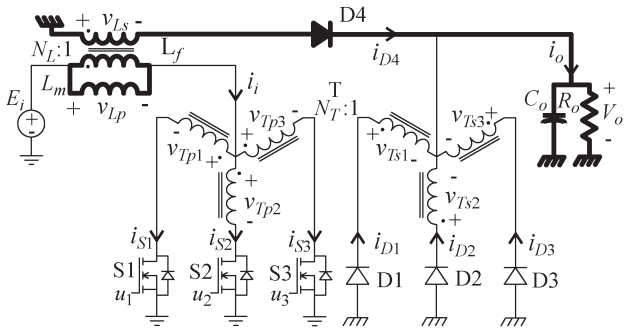

Fig. 4. Equivalent circuit of second stage $[t_1, t_2]$.

2) Second Stage $[t_1, t_2]$*:* The equivalent circuit of this stage is shown in Fig. 4. This stage starts at instant t_1, when the transistor S1 is turned off and D4 is forward biased. The output voltage is applied across the secondary winding of the inductor, and consequently, the induced voltage on the primary winding is $V_{\rm Lp} = -N_LV_o$. The magnetizing current of the inductor flows through D4 ($i_{D4} = N_Li_m$).

Fig. 5 shows the main waveforms in CCM for $N_L = 2N_T$, where the output current has the same shape as the magnetizing current of inductor i_m, since this relationship guarantees the same current amplitude at the output.

B. Static Gain

The expression for the static gain, for a continuous inductor magnetic flux, can be obtained from the analysis of the average voltage across the inductor primary winding

$$V_{\rm Lp} = \frac{1}{T_s}\int_{t_0}^{t_0+T_s} v_{\rm Lp}\,dt = 0 \tag{1}$$

$$(E_i - 2N_TV_o)t_{\rm on} - N_LV_o\left(\frac{T_s}{3} - t_{\rm on}\right) = 0. \tag{2}$$

Rearranging (2), it is possible to obtain

$$\frac{V_o}{E_i} = \frac{3D}{N_L + 3(2N_T - N_L)D}. \tag{3}$$

According to (3), the static gain of the proposed converter is a function of the turn ratios of the inductor and the transformer and the duty cycle D. With N_L and N_T being invariant

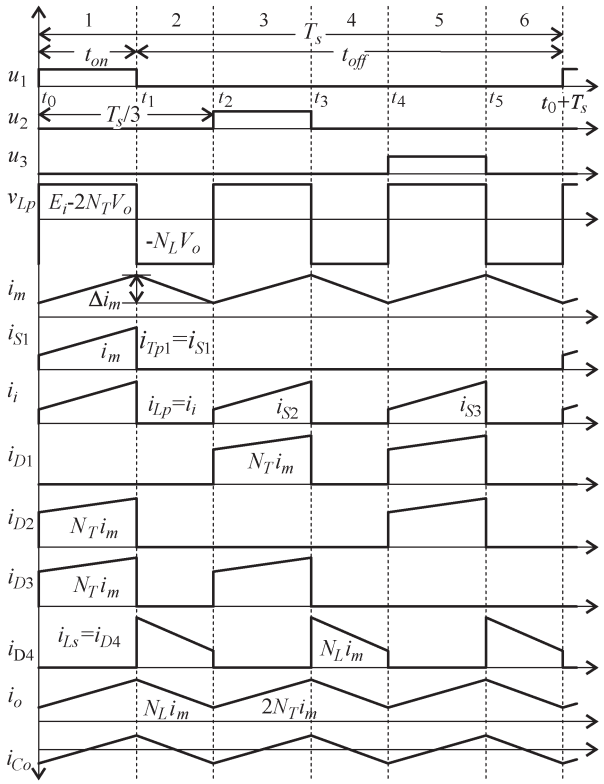

Fig. 5. Main waveforms of the three-phase Weinberg converter for $N_L = 2N_T$.

parameters, the output voltage can be regulated through the duty cycle. However, the static gain is a nonlinear function of it. Thus, by using the relationship $N_L = 2N_T$, it is possible to eliminate the variable D at the denominator of (3)

$$\frac{V_o}{E_i} = \frac{3D}{N_L} = \frac{3D}{2N_T}. \tag{4}$$

Equation (4) shows that the proposed converter presents the static gain of a buck-type converter for $N_L = 2N_T$.

C. Ripple in Magnetizing Current of L_f

The current ripple (ΔI_m) in the magnetizing inductance of the inductor L_f can be obtained from the second stage

$$\Delta I_m = \frac{1}{L_m}\int_{t_0}^{t_1} v_{\mathrm{Lp}}\, dt = \frac{V_o}{L_m}\left(\frac{E_i}{V_o} - 2N_T\right) t_{\mathrm{on}}. \tag{5}$$

The per-unit magnetizing current ripple is given by

$$\overline{\Delta I_m} = \frac{\Delta I_m L_m}{V_o T_s} = \left(\frac{E_i}{V_o} - 2N_T\right) D. \tag{6}$$

Substituting the static gain (4) in (6) and solving the result, (7) is found, referring to the per-unit magnetizing current ripple for $N_L = 2N_T$

$$\overline{\Delta I_m} = \frac{N_L}{3}(1-3D) = \frac{2N_T}{3}(1-3D). \tag{7}$$

D. RMS Currents of L_f

From Fig. 5, the relationship between the average values for the magnetizing and the output currents can be obtained

$$I_m = \frac{I_o}{N_L}. \tag{8}$$

Neglecting the high-frequency current ripple in the inductor and using only its average value (8), the primary and secondary rms currents are given by

$$I_{\mathrm{Lprms}} = I_m\sqrt{3D} \tag{9}$$

$$I_{\mathrm{Lsrms}} = N_L I_m\sqrt{1-3D}. \tag{10}$$

E. Voltage Ripple of C_o

The output voltage ripple due to the capacitor current wave, shown in Fig. 5, is determined by

$$\Delta V_o = \frac{\Delta Q^+}{C_o} = \frac{N_L \Delta I_m T_s}{24 C_o}. \tag{11}$$

The per-unit voltage ripple for $N_L = 2N_T$ is

$$\overline{\Delta V_o} = \frac{\Delta V_o L_m C_o f_s^2}{V_o} = \frac{N_T\overline{\Delta I_m}}{12} = N_T\frac{1-3D}{36}. \tag{12}$$

F. RMS Current of C_o

The output capacitor rms current can be calculated by

$$I_{\mathrm{Crms}} = \frac{N_L \Delta I_m}{2\sqrt{3}} = \frac{N_T \Delta I_m}{\sqrt{3}}. \tag{13}$$

G. RMS Current of T

The rms currents through the primary and secondary windings are computed through

$$I_{\mathrm{Tprms}} = I_m\sqrt{D} \tag{14}$$

$$I_{\mathrm{Tsrms}} = N_T I_m\sqrt{2D}. \tag{15}$$

III. Effects of Parasitic Elements

This section describes the modification of the ideal performance of the proposed converter due to parasitic elements of the magnetic devices; however, to simplify the analysis, the winding resistance values are not included.

The physical representation of the three-phase transformer and its assumed magnetic flux distribution are shown in Fig. 6, where Φ_c is the magnetic flux through the magnetic core, Φ_a is the magnetic flux that links the primary and secondary windings of the same phase but does not link different phase windings, and Φ_l is the leakage flux of one winding.

The mathematical model of the three-phase transformer referred to the primary side is given by

$$[V_T] = [L][\dot{I}_T] \tag{16}$$

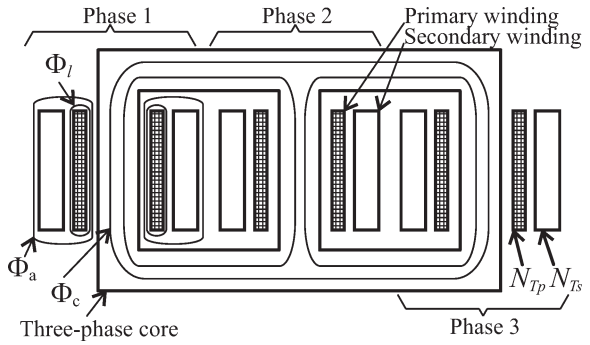

Fig. 6. Three-phase transformer.

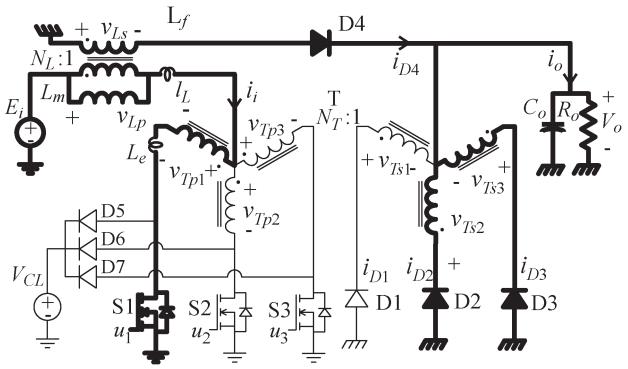

Fig. 7. Equivalent circuit of substage 1a where $l_L = l_{\rm Lp} + l'_{\rm Ls}$ and $L_e = l_{\rm Tp} + 2l'_{\rm Ts} + 3L_{\rm ma}$.

where

$$[V_T]^{\rm T} = [\, v_{\rm Tp1} \quad v_{\rm Tp2} \quad v_{\rm Tp3} \quad v'_{\rm Ts1} \quad v'_{\rm Ts2} \quad v'_{\rm Ts3} \,]$$

$$[I_T]^{\rm T} = [\, i_{\rm Tp1} \quad i_{\rm Tp2} \quad i_{\rm Tp3} \quad i'_{\rm Ts1} \quad i'_{\rm Ts2} \quad i'_{\rm Ts3} \,]$$

$$[L] = L_{\rm mc} \begin{bmatrix} \overline{L_{\rm pp}} & -1/2 & -1/2 & \overline{L_{\rm ps}} & -1/2 & -1/2 \\ -1/2 & \overline{L_{\rm pp}} & -1/2 & -1/2 & \overline{L_{\rm ps}} & -1/2 \\ -1/2 & -1/2 & \overline{L_{\rm pp}} & -1/2 & -1/2 & \overline{L_{\rm ps}} \\ \overline{L_{\rm sp}} & -1/2 & -1/2 & \overline{L_{\rm ss}} & -1/2 & -1/2 \\ -1/2 & \overline{L_{\rm sp}} & -1/2 & -1/2 & \overline{L_{\rm ss}} & -1/2 \\ -1/2 & -1/2 & \overline{L_{\rm sp}} & -1/2 & -1/2 & \overline{L_{\rm ss}} \end{bmatrix}$$

$$\overline{L_{\rm pp}} = (l_{\rm Tp} + L_{\rm ma} + L_{\rm mc})/L_{\rm mc}$$

$$\overline{L_{\rm ss}} = (l'_{\rm Ts} + L_{\rm ma} + L_{\rm mc})/L_{\rm mc}$$

$$\overline{L_{\rm ps}} = \overline{L_{\rm sp}} = (L_{\rm ma} + L_{\rm mc})/L_{\rm mc}.$$

The inductances l, $L_{\rm ma}$, and $L_{\rm mc}$ relate the transformer currents to the flux linkages λ_l, λ_a, and λ_c ($\lambda = N\Phi$). Thus, l is the leakage inductance of a magnetic device winding. The values of l and $L_{\rm ma}$ are lower than that of $L_{\rm mc}$.

A. Operation With Parasitic Elements

In order to provide a description of the operating principle, the clamp circuit shown in Fig. 7 was included, since it is necessary to guarantee a suitable voltage across the transistors.

1) First Stage: The first stage of ideal operation, as shown in Fig. 5, is divided into two substages: 1a and 1b. The equivalent circuit for substage 1a is shown in Fig. 7, while substage 1b is the same equivalent circuit as Fig. 3 shows.

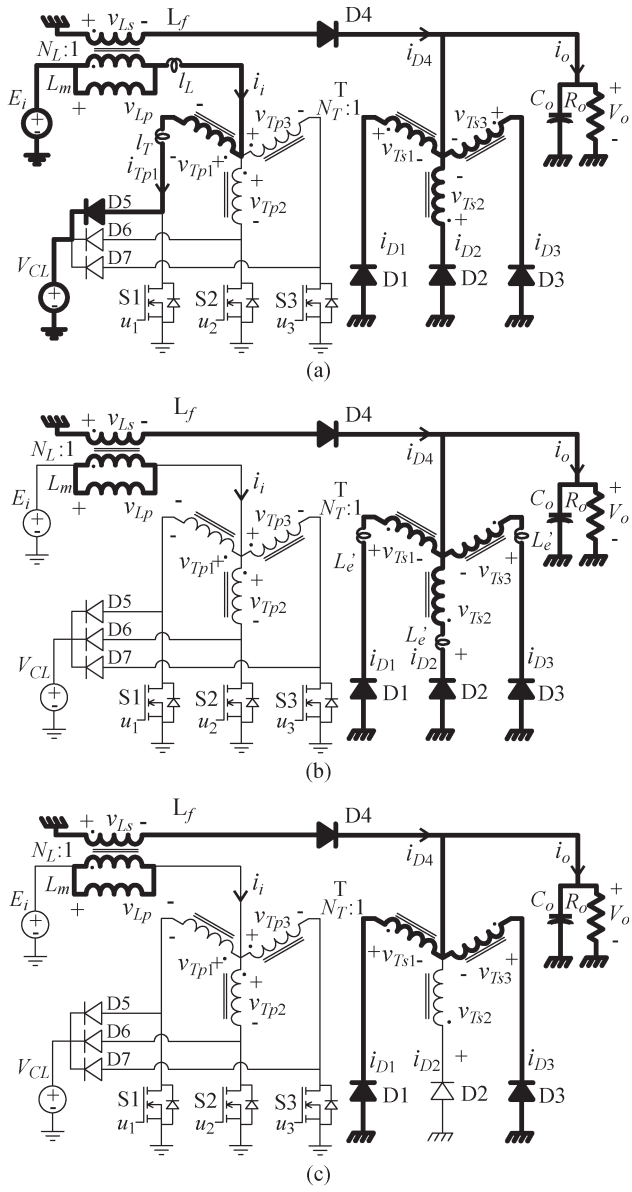

Fig. 8. Equivalent circuits of substages 2a, 2b, and 2c, where $l_T = l_{\rm Tp} + l'_{\rm Ts}$ and $L'_e = l'_{\rm Ts} + L_{\rm ma}$. (a) Substage 2a. (b) Substage 2b. (c) Substage 2c.

In substage 1a, the commutation of semiconductors occurs, and this starts when S1 is turned on at instant t_0. All diodes except D1 are forward biased. The voltage $E_i + N_L V_o$ is applied across the primary winding of phase 1. The inductor magnetizing current commutes from D4 to S1. The current increase across S1 is given by

$$\frac{di_{S1}}{dt} = \frac{E_i + (N_L - 2N_T)V_o}{l_{\rm Lp} + l'_{\rm Ls} + l_{\rm Tp} + 2l'_{\rm Ts} + 3L_{\rm ma}}. \tag{17}$$

2) Second Stage: The second stage, as shown in Fig. 5, is divided into three substages: 2a, 2b, and 2c. The equivalent circuits are shown in Fig. 8.

In substage 2a, the commutation of semiconductors occurs, and this starts when S1 is turned off at instant t_1. The currents of D2 and D3 remain approximately constant. The input current

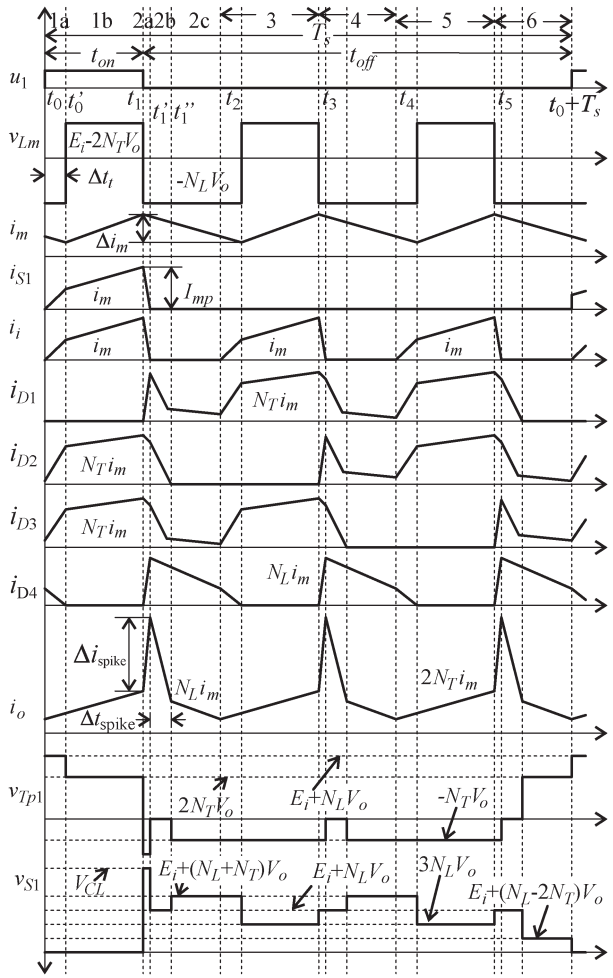

Fig. 9. Main waveforms of the three-phase Weinberg converter, including the effects of parasitic elements of magnetic devices for $N_L = 2N_T$.

falls to zero while the currents of D1 and D4 increase. The input current decrease is determined by

$$\frac{di_i}{dt} = -\frac{V_{\rm CL} - E_i - N_L V_o}{l_{\rm Lp} + l'_{\rm Ls} + l_{\rm Tp} + l'_{\rm Ts}}. \tag{18}$$

In substage 2b, the input current is zero, and the magnetizing current of the inductor flows completely through D4. The energies of the fluxes Φ_{a1}, Φ_{a2}, and Φ_{a3} are transferred to the output side through diodes D1, D2, and D3 whose currents decrease at a rate of

$$\frac{di'_{D1}}{dt} = \frac{di'_{D2}}{dt} = \frac{di'_{D3}}{dt} = -\frac{N_T V_o}{l'_{\rm Ts} + L_{\rm ma}}. \tag{19}$$

Substage 2c starts when flux Φ_{a2} becomes null. D1 and D3 continue to be forward biased because fluxes Φ_{a1} and Φ_{a3} are positive. The rate of these currents is calculated through

$$\frac{di'_{D1}}{dt} = \frac{di'_{D3}}{dt} = -\frac{N_T V_o}{l'_{\rm Ts} + L_{\rm ma} + L_{\rm mc}}. \tag{20}$$

The waveforms of the currents for a switching cycle are obtained by extending the aforementioned analysis to other stages, and these are shown in Fig. 9. The transistor current shows that the transition from off to on is slow. This is due to a large equivalent inductance $L_{\rm eq} = l_{\rm Lp} + l'_{\rm Ls} + l_{\rm Tp} + 2l'_{\rm Ts} + 3L_{\rm ma}$ present during this transition, as can be seen in (17). Moreover, the demagnetizing of inductance L'_e in substage 2b causes a spike in the output current with an amplitude and a time interval given, approximately, in (21) and (22), respectively, where $I_{\rm mp}$ is the peak magnetizing current in L_m

$$\Delta i_{\rm spike} \approx 3N_T I_{\rm mp} \tag{21}$$

$$\Delta t_{\rm spike} \approx \frac{I_{\rm mp}}{N_T V_o} L'_e. \tag{22}$$

B. Static Gain

Fig. 9 shows that the energy storage time of the inductor is affected by the time of transition from off to on when a transistor is switched. Thus, the static gain for $N_L = 2N_T$ is defined by

$$\frac{V_o}{E_i} = \frac{3D}{N_L} - \frac{3\Delta t_t}{N_L T_s} \tag{23}$$

where Δt_t is the time interval in which the current becomes zero across D4 and it can be obtained from (17)

$$\Delta t_t = \frac{I_m}{E_i} L_{\rm eq}. \tag{24}$$

The substitution of (24) in (23) gives (25) which is the static gain in CCM for $N_L = 2N_T$. This equation shows that static gain decreases as a function of the output current

$$\frac{V_o}{E_i} = \frac{3D}{N_L} - \frac{3I_o L_{\rm eq}}{{N_L}^2 E_i T_s}. \tag{25}$$

C. Transistor and Transformer Voltages

The voltage waveforms of the transistor and primary winding of the three-phase transformer are shown in Fig. 9. The voltage across transistors is affected by the transference of the energy stored in the three-phase transformer. Thus, the maximum voltage $V_{\rm Smx}$ across the transistors occurs when all transistors are turned off

$$V_{\rm Smx} = E_i + (N_L + N_T)V_o. \tag{26}$$

For $N_L = 2N_T$, this voltage is

$$V_{\rm Smx} = E_i + 3N_T V_o. \tag{27}$$

IV. Design Example

In this section, a simplified design example of the three-phase Weinberg isolated dc–dc converter is presented using the specifications summarized in Table I. The laboratory prototype is designed to operate as a buck circuit, i.e., for the case of $N_L = 2N_T$, and its purpose is to verify the operation of the converter according to the theoretical description. Therefore, the aim of this design is not to obtain a high-efficiency laboratory prototype. The equations developed for ideal operation are

TABLE I
SPECIFICATIONS OF PROTOTYPE

Parameters		Value
Input voltage (E_i)	:	120 VDC
Output voltage (V_o)	:	75 VDC
Output power (P_o)	:	750 W
Switching frequency (f_s)	:	42 kHz
Current ripple in L_m ($\%\Delta I_m$)	:	25 %
Voltage ripple in C_o ($\%\Delta V_o$)	:	0.5 %

used to compute the voltage and current stresses. The gate drive signals are generated by Kit DSP TMS320LF2407. Nonisolated drive circuits are employed to control the switching transistors.

A. Inductor L_f

A duty cycle of 25% is assumed in order to minimize the input current ripple; thus, the turn ratio for nominal conditions is obtained from (4)

$$N_L = 3D\frac{E_i}{V_o} = 3 \cdot 0.25\frac{120}{75} = 1.2. \tag{28}$$

The average magnetizing current considering a converter efficiency of 95% is computed as

$$I_m = \frac{P_o}{\eta N_L V_o} = \frac{750}{0.95 \cdot 1.2 \cdot 75} = 8.8 \text{ A}. \tag{29}$$

The magnetizing inductance for the specifications given in Table I is obtained through (5) as follows

$$L_m = \frac{75 \cdot 1.2 \cdot (1 - 3 \cdot 0.25)}{3 \cdot 0.25 \cdot 8.8 \cdot 42\,000} = 81\ \mu\text{H}. \tag{30}$$

The primary and secondary rms currents are computed using (9) and (10)

$$I_{\text{Lprms}} = 8.8\sqrt{3 \cdot 0.25} = 7.6 \text{ A} \tag{31}$$

$$I_{\text{Lsrms}} = 8.8 \cdot 1.2\sqrt{1 - 3 \cdot 0.25} = 5.28 \text{ A}. \tag{32}$$

The inductor area product is achieved using the following expression:

$$\begin{aligned} A_e A_w &= \frac{L_m I_{\text{mp}}(I_{\text{Lprms}} + I_{\text{Lsrms}}/N_L)}{J_{\max} B_{\max} k_w} \\ &= \frac{81 \cdot 10^{-6} \cdot 9.9 \cdot (7.6 + 4.4)}{300 \cdot 0.25 \cdot 10^{-4} \cdot 0.4} \\ &= 3.2 \text{ cm}^4 \end{aligned} \tag{33}$$

where $I_{\text{mp}} = I_m(1 + 0.5 \cdot \%\Delta I_L) = 9.9$ A, $J_{\max} = 300$ A/cm^2, $B_{\max} = 0.25$ T, and $k_w = 0.4$ (occupation factor of core window).

B. Three-Phase Transformer T

The turn ratio N_T is determined as

$$N_T = \frac{N_L}{2} = \frac{1.2}{2} = 0.6. \tag{34}$$

TABLE II
LIST OF POWER DEVICES

Component		Description
Inductor	:	Core EE-55/28/25
		Primary: 6 turns, 16x25AWG, 6 mΩ
		Secondary: 5 turns, 9x25AWG, 9 mΩ
		$L_m = 79\mu$H, $l_L = 0.6\ \mu$H
3ϕ transformer	:	Core EE-66/33/39
		Primary: 6 turns, 4x21AWG, 18 mΩ
		Secondary: 10 turns, 5x21AWG, 24 mΩ
		$l_T = 0.9\ \mu$H, $L_e = 11.1\ \mu$H
Capacitor	:	2/EPCOS B43501
		1000 μF/ 250 V
Transistors	:	Cool-MOS/SPP20N60S5
		600 V/20 A/0.19 Ω
Diodes	:	SiC-Schottky/SDT10S60
		600 V/10 A/1.7 V

The primary and secondary rms currents are calculated through (14) and (15), respectively

$$I_{\text{Lprms}} = 8.8\sqrt{0.25} = 4.4 \text{ A} \tag{35}$$

$$I_{\text{Lsrms}} = 0.6 \cdot 8.8\sqrt{2 \cdot 0.25} = 3.7 \text{ A}. \tag{36}$$

The transformer area product is obtained using the following expression:

$$\begin{aligned} A_e A_w &= \frac{2N_T V_o}{3 f_s J_{\max} 2B_{\max} k_w}\left(2I_{\text{Tprms}} + 2\frac{I_{\text{Tsrms}}}{N_T}\right) \\ &= \frac{2 \cdot 0.6 \cdot 75 \cdot 10}{3 \cdot 42 \cdot 300 \cdot 0.50 \cdot 0.3}\left(2 \cdot 4.4 + 2\frac{3.7}{0.6}\right) \\ &= 3.35 \text{ cm}^4. \end{aligned} \tag{37}$$

C. Filter Capacitor

Electrolytic capacitors are used as the output filter capacitor. The values for the capacitance and rms current are computed using (11) and (13), respectively

$$C_o = \frac{1.2 \cdot 0.25 \cdot 8.8}{24 \cdot 42\,000 \cdot 0.005 \cdot 75} = 7.0\ \mu\text{F} \tag{38}$$

$$I_{\text{Crms}} = \frac{1.2 \cdot 0.25 \cdot 8.8}{2\sqrt{3}} = 0.76 \text{ A}. \tag{39}$$

D. List of Power Devices

Table II lists the prototype power devices. The resistance values for the inductor and transformer are calculated while their inductance values are measured. The schematic circuit of the laboratory prototype of the three-phase Weinberg isolated dc–dc converter is shown in Fig. 10.

E. Power Losses

The power losses due to resistances and voltage drops in the circuit are listed in Table III. The transistor turn-off losses are also included, where a clamp voltage V_{CL} of 400 V and a fall

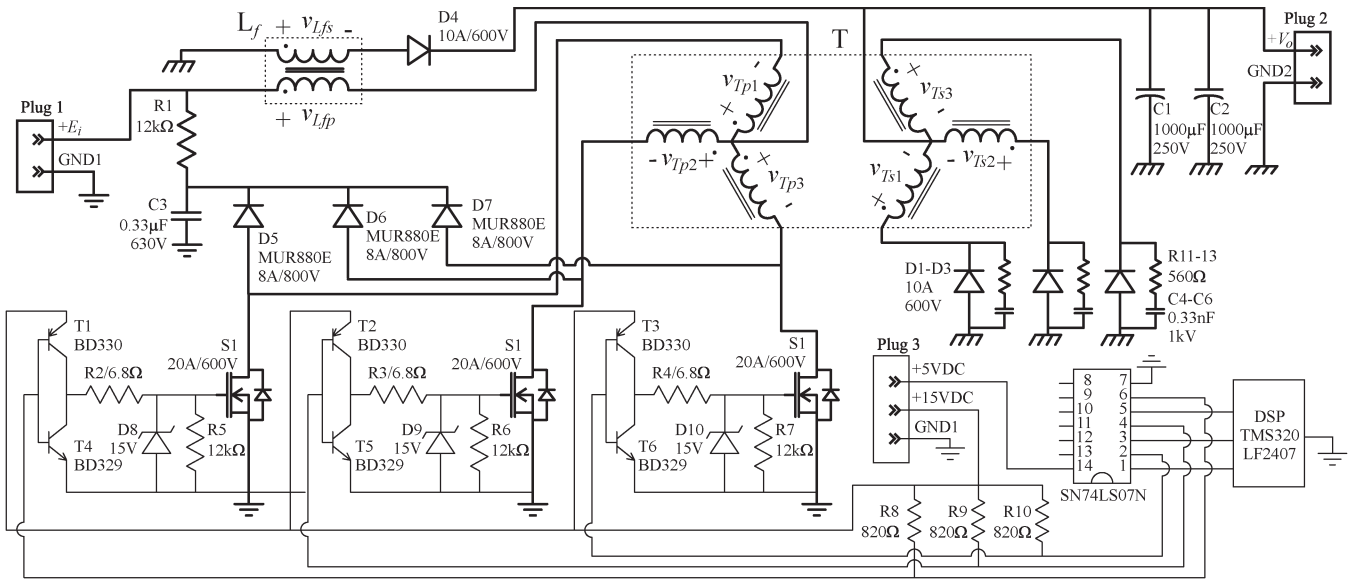

Fig. 10. Schematic circuit of the implemented laboratory prototype.

TABLE III
POWER LOSSES

Component		Equation	Value
Transistors	:	$3 \cdot {I_{Tprms}}^2 R_{on}$	11.0 W
		$3V_{CL}I_{mp}t_f f_s/2$	7.5 W
Diodes	:	$I_o \cdot V_F$	17.0 W
Inductor	:	${I_{Lprms}}^2 R_{Lp} + {I_{Lsrms}}^2 R_{Ls}$	0.5 W
Transformer	:	$3{I_{Tprms}}^2 R_{Tp} + 3{I_{Tsrms}}^2 R_{Ls}$	2.0 W
Total	:		38 W

time t_f of 30 ns were considered. The turn-on losses are not included due to soft switching. Thus, the expected efficiency is computed as

$$\eta = \frac{P_o}{P_i} = \frac{750}{750 + 38} = 95.2\%. \tag{40}$$

V. EXPERIMENTAL RESULTS

Figs. 11 and 12 show the input, transistor, output, and diode currents for an input voltage of 120 Vdc, an output voltage of 75 Vdc, an output load of 735 W, and a duty cycle of 29.2%. The figures show that the input and output currents are evenly distributed through the transistors and diodes and that the frequency of these currents is three times the switching frequency. Fig. 11 also shows that the switching of the transistor at turn-on is soft and at turn-off is hard. The output current shape of the measured waveform is similar to that of the theoretical waveform shown in Fig. 9; therefore, the amplitude and the time interval of the spike current can be calculated by (21) and (22), respectively, where $L'_e \approx L_e/3$ is assumed. These values match closely the experimental results

$$\Delta i_{\text{spike}} \approx 3N_T I_{\text{mp}} = 3 \cdot 0.6 \cdot 9.9 = 17.8 \text{ A}$$

$$\Delta t_{\text{spike}} \approx \frac{I_{\text{mp}}}{N_T V_o} L'_e = \frac{9.9}{0.6 \cdot 75} 3.7 \cdot 10^{-6} = 0.81 \ \mu\text{s}.$$

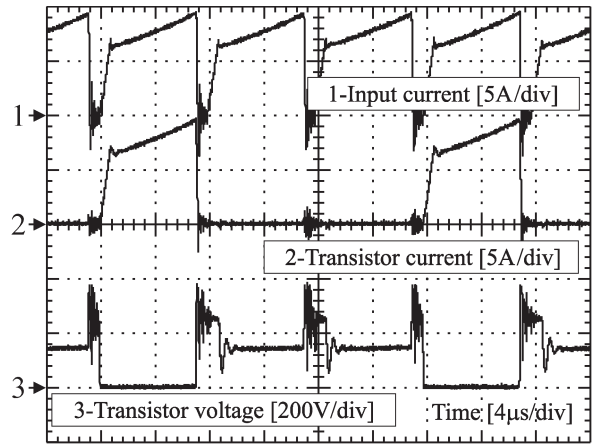

Fig. 11. Input and transistor S1 currents and transistor S1 voltage for $D = 0.292$, $E_i = 120$ V, $V_o = 75$ V, and $P_o = 735$ W.

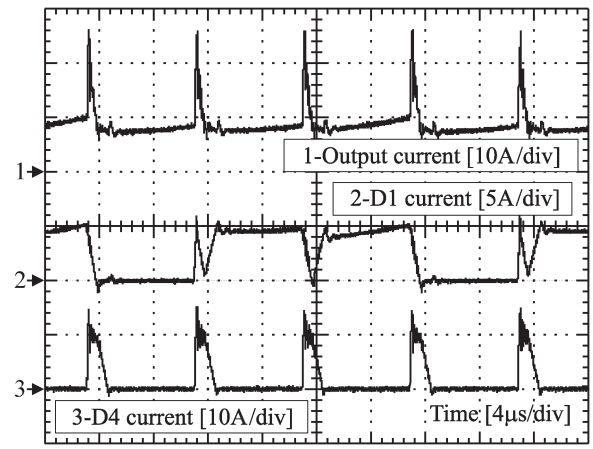

Fig. 12. Output, diode D1, and diode D4 currents for $D = 0.292$, $E_i = 120$ V, $V_o = 75$ V, and $P_o = 735$ W.

Fig. 13 shows the output voltage and voltage waveforms across the primary windings of the transformer and the inductor.

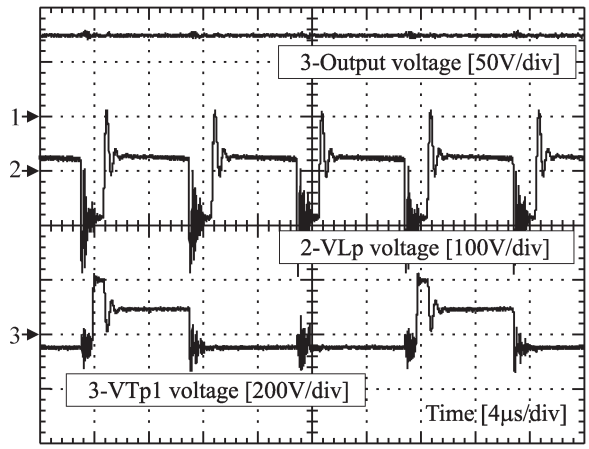

Fig. 13. Output voltage, primary voltage of L_f, and primary voltage of T for $D = 0.292$, $E_i = 120$ V, $V_o = 75$ V, and $P_o = 735$ W.

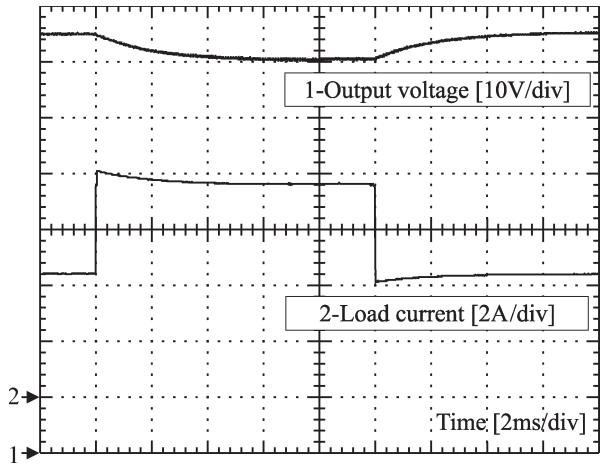

Fig. 14. Step load response in open-loop control.

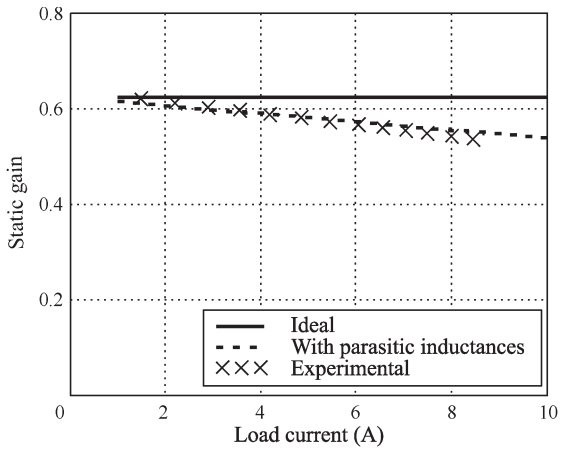

Fig. 15. Static gain in CCM of the laboratory prototype for input voltage of 120 V and duty cycle of 25%.

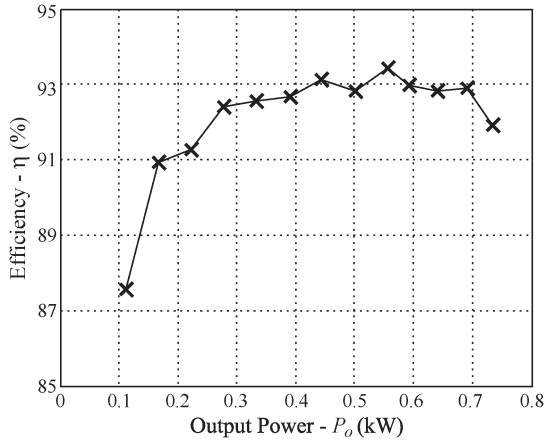

Fig. 16. Measured efficiency of the laboratory prototype.

Fig. 14 shows the output voltage response for a step load change in open-loop control. This response was obtained for an input voltage of 120 V and a duty cycle of 26.1%. The step load was achieved by changing the load resistance from 17 to 9.2 Ω, and it represents an increase of 112% in the initial load power. The performance shows that the converter has a first-order response, and thus, a simple proportional–integral controller can be used when a regulated output voltage is required.

Fig. 15 shows the static gain of the laboratory prototype with the ideal curve and that which considers parasitic elements given in (25), where the equivalent inductance $L_{\rm eq}$ is 11.7 μH, which is obtained from Table II.

The measured efficiency of the laboratory prototype is shown in Fig. 16. The curve was obtained keeping the input and output voltages constant (120-V input and 75-V output). The curve shows that the laboratory prototype does not have a good efficiency; however, it can be considered suitable since the components are not optimized. For example, further reduction in the forward voltage drop of the diode can bring higher efficiency but with increased costs.

VI. Conclusion

A three-phase Weinberg isolated dc–dc converter, which combines the main characteristics of the Weinberg and the three-phase dc–dc converters, has been presented herein. The proposed converter allows an increase in the operation frequency of the filters to three times the switching frequency, resulting in small and lightweight filters. Furthermore, the use of a nonisolated gate drive is allowed since the transistors are connected to the same reference point. The current-fed sourcing provides high impedance at the input side, and thus, the three-phase transformer does not present the flux-imbalance problem due to asymmetry in the volt–second product applied between its phases. The input and output current ripples are cancelled for a duty cycle of 1/3 or 2/3. These characteristics make the proposed converter suitable for applications such as in power conversion systems for telecommunication, electric vehicles, renewable energy systems, and battery chargers.

References

[1] A. H. Weinberg, "A boost regulator with a new energy-transfer principle," in *Proc. Spacecraft Power Conditioning Electron. Semin.*, Sep. 1974, pp. 155–122.

[2] P. W. Clarke, "Converter regulation by controlled conduction overlap," U.S. Patent 3 938 204, Feb. 10, 1976.

[3] V. J. Thottuvelil, T. G. Wilson, and H. A. Owen, Jr., "Analysis and design of a push–pull current-fed converter," in *Proc. Power Electron. Spec. Conf.*, 1981, pp. 192–203.

[4] R. Redl and N. O. Sokal, "Push–pull current-fed multiple-output regulated wide-input-range DC/DC power converter with only one inductor and

with 0% to 100% switch duty ratio: Operation at duty ratio below 50%," in *Proc. Power Electron. Spec. Conf.*, 1981, pp. 204–212.
[5] Q. Li and P. Wolfs, "A review of the single phase photovoltaic module integrated converter topologies with three different dc link configurations," *IEEE Trans. Power Electron.*, vol. 23, no. 3, pp. 1320–1333, May 2008.
[6] S. K. Mazumder, K. Acharya, and C. M. Tan, "Design of an all-SiC parallel dc/dc Weinberg converter unit using RF control," *IEEE Trans. Power Electron.*, vol. 23, no. 6, pp. 2893–2904, Nov. 2008.
[7] J.-M. Kwon, E.-H. Kim, B.-H. Kwon, and K.-H. Nam, "High-efficiency fuel cell power conditioning system with input current ripple reduction," *IEEE Trans. Ind. Electron.*, vol. 56, no. 3, pp. 826–834, Mar. 2009.
[8] F. H. Khan, L. M. Tolbert, and W. E. Webb, "Hybrid electric vehicle power management solutions based on isolated and nonisolated configurations of multilevel modular capacitor-clamped converter," *IEEE Trans. Ind. Electron.*, vol. 56, no. 8, pp. 3079–3095, Aug. 2009.
[9] M. Delshad and B. Fani, "A new active clamping soft switching Weinberg converter," in *Proc. ISIEA*, Oct. 4–6, 2009, pp. 910–913.
[10] M. Nymand and M. A. E. Andersen, "High-efficiency isolated boost DC–DC converter for high-power low-voltage fuel-cell applications," *IEEE Trans. Ind. Electron.*, vol. 57, no. 2, pp. 505–514, Feb. 2010.
[11] M. Mohr, W. T. Franke, B. Wittig, and F. W. Fuchs, "Converter systems for fuel cells in the medium power range—A comparative study," *IEEE Trans. Ind. Electron.*, vol. 57, no. 6, pp. 2024–2032, Jun. 2010.
[12] C.-S. Leu and M.-H. Li, "A novel current-fed boost converter with ripple reduction for high-voltage conversion applications," *IEEE Trans. Ind. Electron.*, vol. 57, no. 6, pp. 2018–2023, Jun. 2010.
[13] R. W. De Doncker, D. M. Divan, and M. H. Kheraluwala, "A three-phase soft-switched high-power-density dc/dc converter for high-power applications," *IEEE Trans. Ind. Appl.*, vol. 27, no. 1, pp. 63–73, Jan./Feb. 1991.
[14] P. D. Ziogas, A. R. Prasad, and S. Manias, "Analysis and design of a three phase off-line DC/DC converter with high frequency isolation," *IEEE Trans. Ind. Appl.*, vol. 28, no. 4, pp. 824–832, Jul./Aug. 1992.
[15] D. S. Oliveira, Jr. and I. Barbi, "A three-phase ZVS PWM dc/dc converter with asymmetrical duty cycle for high power applications," *IEEE Trans. Power Electron.*, vol. 20, no. 2, pp. 370–377, Mar. 2005.
[16] S. V. G. Oliveira and I. Barbi, "A three-phase step-up DC–DC converter with a three-phase high frequency transformer," in *Proc. ISIE*, Jun. 20–23, 2005, vol. 2, pp. 571–576.
[17] C. Liu, A. Johnson, and J.-S. Lai, "A novel three-phase high-power soft-switched DC/DC converter for low-voltage fuel cell applications," *IEEE Trans. Ind. Appl.*, vol. 41, no. 6, pp. 1691–1697, Nov./Dec. 2005.
[18] G. Franceschini, E. Lorenzani, M. Cavatorta, and A. Bellini, "3boost: A high-power three-phase step-up full-bridge converter for automotive applications," *IEEE Trans. Ind. Electron.*, vol. 55, no. 1, pp. 173–183, Jan. 2008.
[19] H. Cha, J. Choi, and P. N. Enjeti, "A three-phase current-fed dc/dc converter with active clamp for low-dc renewable energy sources," *IEEE Trans. Power Electron.*, vol. 23, no. 6, pp. 2784–2793, Nov. 2008.
[20] L. Palma, M. H. Todorovic, and P. N. Enjeti, "Analysis of common mode voltage in utility-interactive fuel cell power conditioners," *IEEE Trans. Ind. Electron.*, vol. 56, no. 1, pp. 20–27, Jan. 2009.
[21] R. L. Andersen and I. Barbi, "A three-phase current-fed push–pull dc–dc converter," *IEEE Trans. Power Electron.*, vol. 24, no. 2, pp. 358–368, Feb. 2009.
[22] D. Vinnikov and I. Roasto, "Quasi-Z-source-based isolated dc/dc converters for distributed power generation," *IEEE Trans. Ind. Electron.*, vol. 58, no. 1, pp. 192–201, Jan. 2011.

Hugo R. E. Larico was born in Arequipa, Peru, in 1980. He received the B.S. degree in electrical engineering from the National University of San Agustin, Arequipa, in 2004 and the M.S. degree in electrical engineering from the Federal University of Santa Catarina (UFSC), Florianópolis, Brazil, in 2007, where he is currently working toward the Ph.D. degree in the Department of Electrical Engineering.

His research interests include design, modeling, control, and simulation of static power conversion systems.

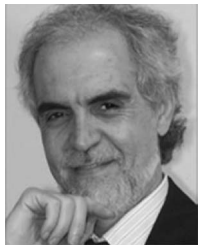

Ivo Barbi (M'76–SM'90–F'11) was born in Gaspar, Brazil, in 1949. He received the B.S. and M.S. degrees in electrical engineering from the Federal University of Santa Catarina (UFSC), Florianópolis, Brazil, in 1973 and 1976, respectively, and the Ph.D. degree from Institut National Polytechnique de Toulouse, Toulouse, France, in 1979.

He is currently a Professor with the Power Electronics Institute (INEP), UFSC. He is the Founder of the Brazilian Power Electronics Society (SOBRAEP) and INEP, UFSC.